ELSEVIER

Journal of Alloys and Compounds 427 (2007) 18–24

Journal of ALLOYS AND COMPOUNDS

www.elsevier.com/locate/jallcom

Hydrogen self-dynamics in orthorhombic alkaline earth hydrides through incoherent inelastic neutron scattering

D. Colognesi [a,*], G. Barrera [b], A.J. Ramirez-Cuesta [c], M. Zoppi [a]

[a] *Consiglio Nazionale delle Ricerche, Istituto dei Sistemi Complessi, Sezione di Firenze, via Madonna del Piano 10, 50019 Sesto Fiorentino (FI), Italy*
[b] *Departamento de Química, Universidad Nacional de la Patagonia SJB, Ciudad Universitaria, 9005 Comodoro Rivadavia, Argentina*
[c] *ISIS facility, Rutherford Appleton Laboratory, Chilton, Didcot, OX11 0QX, United Kingdom*

Received 8 February 2006; received in revised form 6 March 2006; accepted 8 March 2006
Available online 18 April 2006

Abstract

Inelastic neutron scattering patterns from polycrystalline CaH_2, SrH_2 and BaH_2, measured on TOSCA-II spectrometer at low temperature in the energy transfer range $3\,meV < E < 500\,meV$ are reported. From the medium-energy regions, coinciding with optical phonon bands, high-quality generalized self-inelastic structure factors are extracted and compared to new ab initio lattice dynamics simulations, accurately reproducing the hydride lattice structures. The overall agreement is found satisfactory, even though not perfect, especially in the first optical phonon zone of BaH_2. In addition, the simulations provide a compelling support to a recent physical interpretation of the recorded spectral features and allowed to separate the contributions produced by the two non-equivalent hydrogen atoms.

Keywords: Metal hydrides; Neutron scattering; Lattice dynamics

1. Introduction

Ionic hydrides have gained a new wave of interest in the last years, mainly in connection with the hydrogen storage problem, where, for example, sodium aluminum tetrahydride [1] seems to play an important role. As a result several studies on magnesium dihydride have been recently accomplished, both experimentally and theoretically, including Raman and incoherent inelastic neutron scattering measurements [2], ab initio electronic and lattice dynamics simulations [3], and even high-pressure neutron diffraction [4]. However, differently from alkali hydrides, which exhibit the same ambient-pressure structure [5] along the group I moving from lithium to cesium, alkaline earth hydrides are characterized by three distinct subsets: BeH_2, unstable and body-centered orthorhombic with an *Ibam* space group [6], MgH_2, well-described and showing a rutile-type structure (tetragonal, $P4_2/mnm$) a low pressure [5], and, finally, calcium, strontium and barium dihydrides, isomorphic and crystallizing with an orthorhombic lattice (at low pressure and temperatures below 600 °C), exhibiting the *Pnma* space group.

These three Heavy Alkaline Earth Hydrides (labeled $HAEH_2$ in short) were structurally studied for the first time in 1935 [7], when the metal atom position was determined through standard X-ray powder diffraction: alkaline earth atoms appeared arranged in a slightly-distorted hexagonal close-packed structure, as shown in Fig. 1a. On the other hand, the hydrogen locations were not resolved and so the H atoms were assumed to occupy two four-fold positions in *4(c)* sites: one in the center of octahedral holes, and the other in the center of triangles created by metal atoms and forming the common base of two tetrahedra. From Fig. 1b it can be seen that H atoms fall into line along the *z*-coordinate direction. However, further neutron scattering experiments on deuterated powder samples (CaD_2 [8], SrD_2 [9] and BaD_2 [10]) showed the hydrogen locations suggested by Zintl and Harder [7] to be incompatible with the new diffraction data, and a slightly-distorted $PbCl_2$-type structure was proposed for the three $HAEH_2$ (see Fig. 2). Finally, recent X-ray single-crystal measurements on CaD_2 and SrD_2 [11], and on BaH_2 [12] basically confirmed the neutron scattering findings, with minor differences in the values of the *z* coordinate for the H/D(1) atom and of the *x* coordinate for the H/D(2) atom.

* Corresponding author. Tel.: +39 055 5226681; fax: +39 055 5226683.
E-mail address: daniele.colognesi@fi.isc.cnr.it (D. Colognesi).

0925-8388/$ – see front matter © 2006 Elsevier B.V. All rights reserved.
doi:10.1016/j.jallcom.2006.03.031

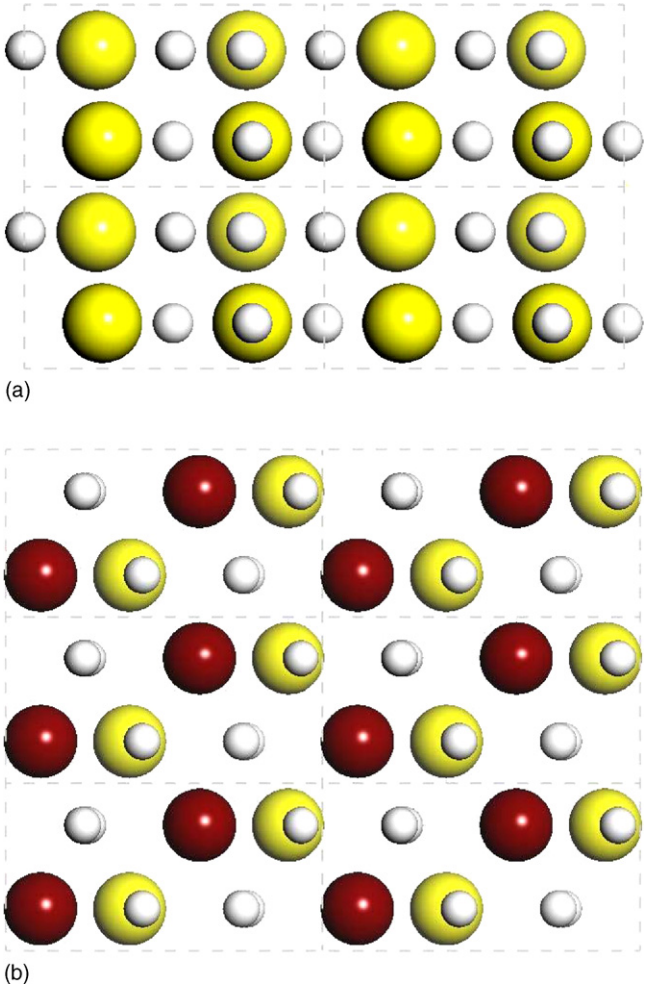

Fig. 1. Crystal structure of CaH_2 as proposed by Zintl and Harder [7], where H atoms are represented by small white balls, and calcium atoms by large yellow or red balls (different colors label different heights). In panel (a) the *y*-axis is perpendicular to the paper, while *x* and *z* are horizontal and vertical, respectively. In panel (b) the *x*-axis is perpendicular to the paper, while *y* and *z* are horizontal and vertical, respectively.

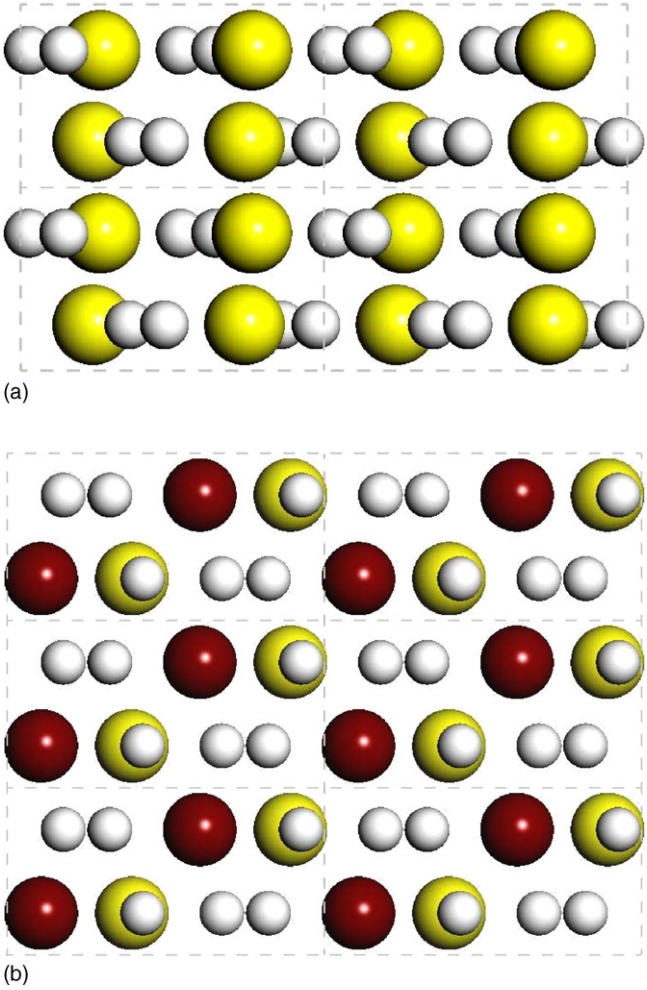

Fig. 2. Crystal structure of CaH_2 as proposed by Bergsma and Loopstra [8], where H atoms are represented by small white balls, and calcium atoms by large yellow or red balls (different colors label different heights). In panel (a) the *y*-axis is perpendicular to the paper, while *x* and *z* are horizontal and vertical, respectively. In panel (b) the *x*-axis is perpendicular to the paper, while *y* and *z* are horizontal and vertical, respectively.

If the situation concerning the microscopic structure of $HAEH_2$ can be considered nowadays as quite satisfactory, this is not at all the case about their lattice dynamics, where only two experimental studies have been so far reported, both making use of the Incoherent Inelastic Neutron Scattering (IINS) technique in order to extract the hydrogen vibrational spectra. However, while one work [13] shows good quality data from CaH_2 at temperatures of 10 and 295 K, the other, which had the ambition to explore the complete series of $HAEH_2$ [14], offers only low-resolution spectra in a narrow energy transfer range (400–1250 cm^{-1}), due to the limitations of the neutron equipment of that time. For this reason the present study will report new incoherent inelastic measurements on all the $HAEH_2$ using a modern neutron spectrometer, which exhibits both good energy resolution and wide energy transfer range.

Finally, if one considers the first-principles simulations of the $HAEH_2$ properties, the present scenario also looks rather unsatisfactory. Only two groups have devoted some effort to this class of compounds: El-Gridani and various coworkers have simulated the elastic, electronic and structural properties of CaH_2 [15,16], SrH_2 [17] and BaH_2 [18] making use of the Hartee-Fock or the pseudopotential method in connection with the CRYSTAL95 program, while Smithson et al. [19] studied the stability and electronic structure of all the metal hydrides (including of course $HAEH_2$) through the VASP simulation package. However, no information on the lattice dynamics was reported by either groups. A closer look to refs. [15,16,18] made clear that these electronic band calculations were all performed using initial lattice structures taken from ref. [7] (i.e. not the most recently measured), optimizing the cell parameters (three degrees of freedom) and the internal coordinates (six degrees of freedom) in separate sub-runs. In this way the final lattice structures obtained from the reported ab initio calculations are not, generally speaking, the most stable. In addition, the calculations on SrH_2 [17] and BaH_2 [18] were set up simply considering the $(n-1)s$ and $(n-1)p$ electrons as part of the core, so that the reported results should be analyzed with some caution. This inadequate situation prompted the authors of the present work to develop independent

ab initio lattice dynamics simulations in order to check the residual structural ambiguities of $HAEH_2$ and, moreover, to extract the phonon spectra to be compared with the experimental neutron results. Besides, in order to assess the importance of the $(n-1)s$ and $(n-1)p$ electrons in the bonding of these solids, electronic structure calculations were carried out both considering the $(n-1)s$ and $(n-1)p$ electrons as part of the core, and as semi-core electrons built in the appropriate pseudopotentials.

The rest of the paper will be organized as follows: experimental IINS procedure and spectral data analysis will be shortly described Section 2, while Section 3 will be devoted to a brief explanation of the ab initio simulations. In Section 4 we will discuss the experimental results in comparison with the simulation ones. Finally, Section 5 will contain the conclusions of the present study.

2. Experimental procedure and data analysis

The IINS measurements were carried out using TOSCA-II [20], a crystal-analyzer inverse-geometry spectrometer operating at the ISIS pulsed neutron source (Rutherford Appleton Laboratory, UK). This instrument covers an extended energy transfer, E, range: 3 meV $< E <$ 500 meV, providing an excellent energy resolution, ΔE, ($\Delta E/E \cong$ 1.5–3%). However, because of the fixed detector geometry and the small value of the final neutron energy, E_1, the wave-vector transfer, Q, is rigidly determined by E, being roughly proportional to the square root of the incoming neutron energy, E_0. The three hydride samples, all in the form of polycrystalline powder and purchased from Johnson Matthey GmbH Alfa (CaH_2 and BaH_2) and Chemos GmbH (SrH_2), were loaded into flat aluminum cells (size: 34 mm × 48 mm, with 1 mm thick walls and 5 mm of internal gap). Special care was devoted to prevent possible alkaline earth hydroxide formation by working in an inert-gas glove box. Then the loaded cells were placed into the TOSCA-II closed-cycle refrigerator at $T = 20.0(3)$ K (except SrH_2, kept at $T = 16.0(3)$ K) for the actual IINS measurements. An additional empty cell run was also performed. In Table 1 we have summarized all the various experimental details concerning the three alkaline earth hydride samples.

The experimental back-scattering time-of-flight data were transformed into double-differential cross-section spectra, detector by detector, making use of the standard instrumental routines, and finally added together in a single data block. This measurement was corrected for the $(E_1/E_0)^{1/2}$ kinematic factor and then the empty-can contribution was properly subtracted [21], taking into account the E_0-dependent sample transmission. At this stage the important corrections for self-absorption attenuation and multiple scattering contamination were performed through the analytical approach suggested by Agrawal and Sears in the case of a flat slab-like sample [22]. Both procedures were carried out in the framework of the incoherent approximation [23], totally justified by the preponderance of scattering from the H nuclei and by the polycrystalline nature of the hydrides. Making use of the method explained in ref. [24], the inputs needed for these two corrections were reduced to the knowledge of the atom-projected density of phonon states, which were approximately set up using the procedure reported in details in refs. [25,26].

Multiple scattering contributions containing two or more inelastic scattering events were found to be modest (but not negligible) in the energy transfer interval of interest (i.e. 3 meV $< E <$ 150 meV, the range of the fundamental bands),

Table 1
Sample description, including experimental temperature T, integrated proton current IPC, mass, sample scattering power p (at $E = 100$ meV), and purity

Sample	T (K)	IPC (μA h)	Mass (g)	p (%)	Purity (wt.%)
CaH_2	20.0(3)	1828.9	3.94	16.98	98
SrH_2	16.0(3)	3248.1	6.06	12.65	99.5
BaH_2	20.0(3)	2551.9	6.40	8.12	99.5
Empty	20.0(3)	895.8	–	–	–

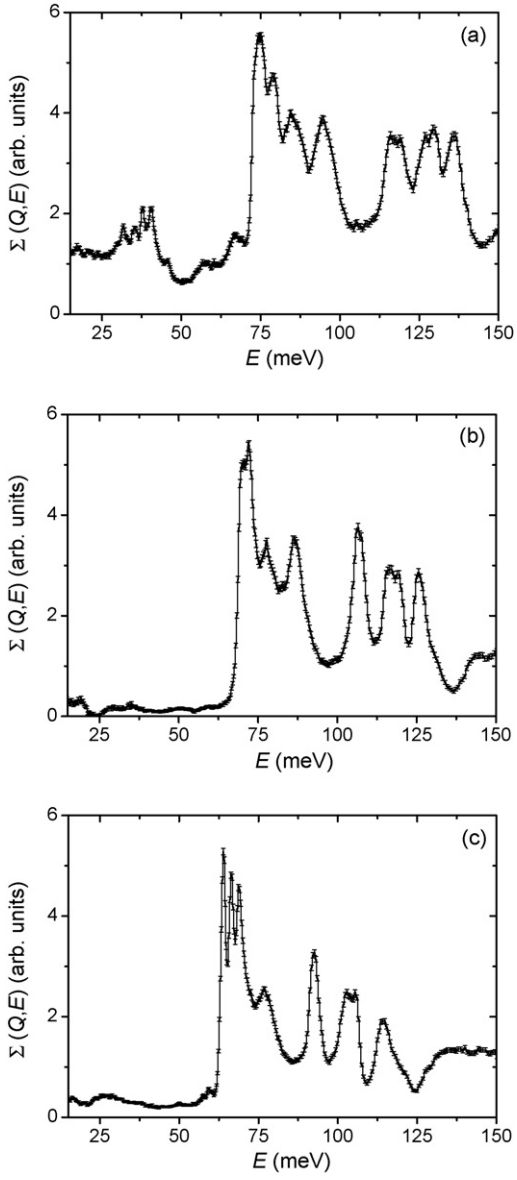

Fig. 3. Generalized self-inelastic structure factor from CaH_2 (a); SrH_2 (b); and BaH_2 (c) recorded in back-scattering at $T \leq 20$ K.

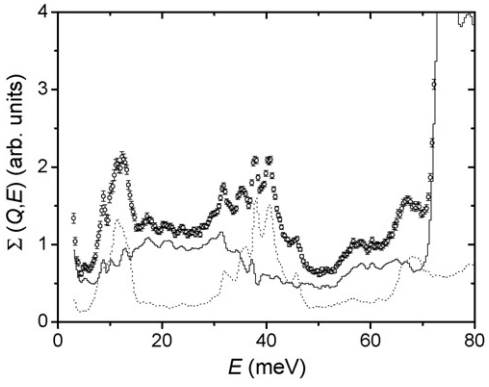

Fig. 4. Detail of the $Ca(OH)_2$ contamination in the generalized self-inelastic structure factor from CaH_2: experimental CaH_2 data from Fig. 3a (circles with error bars), experimental pure $Ca(OH)_2$ spectrum (dotted line), difference (full line).

amounting on average to 10.5, 6.9 and 4.0% of the total neutron counts for CaH_2, SrH_2 and BaH_2, respectively. Finally these estimates were removed from the processed neutron spectra, which are reported in Fig. 3 in the form of the well-known generalized self-inelastic structure factors, $\Sigma(Q,E)$ [27].

By inspecting the $\Sigma(Q,E)$ spectrum from CaH_2 in Fig. 3a, some clear $Ca(OH)_2$ contaminations have been detected, similarly to what was observed in ref. [13], being some hydroxide probably already present in the commercial hydride samples (Fig. 4). These unwanted features were removed making use of a previous IINS measurement on $Ca(OH)_2$ [28]. As for SrH_2, no sign of hydroxide contamination was observed in the low-energy zone; and finally, concerning the last hydride (i.e. BaH_2), its spectrum showed only a very weak hump in the $25\,meV < E < 37\,meV$ range, probably revealing a negligible barium hydroxide contamination (see Fig. 3c).

3. First-principle simulation

As already mentioned in the introductory section and shown in Fig. 2, the alkaline earth hydrides structure is primitive orthorhombic (space group *Pnma*) with four alkaline earth atoms per unit cell. Both alkaline earth and hydrogen atoms occupy the special symmetry positions *4(c)* at (x, 1/4, z) with different values of x and z for the metal and the two non-equivalent hydrogen atoms. Thus, there are three external (the a, b, and c lattice parameters) and six internal coordinates that have to be specified in order to determine the full crystal structure (reported in Table 2).

Ab initio calculations were carried out using plane-wave density functional theory as implemented by the computer code ABINIT [29] in conjunction with the Hartwigsen-Goedecker-Hutter pseudopotentials [30]. As for the type of density functional employed, the Generalized Gradient Approximation (GGA) has been preferred, using the parameterization introduced by Perdew, Burke and Ernzerhof [31]. The reasons for this choice can be found in refs. [26,32], where it is shown that standard energy minimization methods using GGA give an adequate lattice geometry although the computationally-prohibitive thermal and zero point effects are not included. In addition, as the $(n-1)s$ and $(n-1)p$ electrons are known to be important for the alkaline earth elements, semi-core electrons were explicitly considered in the appropriate pseudopotentials (see Table 3).

The convergence achievement was verified with respect to both the number of k-points in reciprocal space and the energy cut-off for the plane waves: most electronic calculations were performed using a mesh of $4 \times 4 \times 4$ points in the k-space and a cut-off at 1360.72 eV. In order to calculate well-defined densities of phonon states for $HAEH_2$, phonons were determined on a $16 \times 16 \times 16$ grid of points in the first Brillouin zone. However, a full electronic calculation on such a grid was not necessary since an accurate interpolation procedure through the ANADDB [33] program was used. Finally, the actual IINS spectra were generated using the ACLIMAX code [34], which takes exactly into accounts thermal and powder-average effects, together with overtones and combinations up to the tenth quantum event. Simulated generalized self-inelastic structure factors, $\Sigma(Q,E)$, are reported in Fig. 5 (together with their respective fundamental components) after a small rigid shift of the whole phonon frequency sets, namely 3.5, 3.05 and 7.5 meV, respectively, for CaH_2, SrH_2 and BaH_2. In this figure there are also plotted the experimental determinations of the various $\Sigma(Q,E)$ spectra after removing a modest linear background (probably due to some residual sample-dependent spurious scattering) and applying proper scaling constants.

Table 2
Calculated ("GGA") and experimental ("Exp.") values [8,10,11] of the lattice parameters for CaH_2, SrH_2 and BaH_2

	CaH_2		SrH_2		BaH_2	
	GGA	Exp. [8]	GGA	Exp. [11]	GGA	Exp. [10]
a (Å)	5.899	5.925(1)	6.354	6.361(2)	6.812	6.789(1)
b (Å)	3.570	3.581(1)	3.854	3.857(2)	4.150	4.171(1)
c (Å)	6.769	6.776(1)	7.286	7.303(4)	7.836	7.852(1)
x[Met.]	0.23938	0.238(1)	0.26083	0.2607(4)	0.26090	0.260(3)
x[H(1)]	0.35560	0.3573(6)	0.64484	0.63(1)	0.64500	0.655(3)
x[H(2)]	0.97414	0.9737(9)	0.02635	0.05(1)	0.02812	0.029(3)
z[Met.]	0.11030	0.1071(8)	0.88930	0.8895(4)	0.88766	0.887(3)
z[H(1)]	0.42755	0.4269(7)	0.92759	0.92(1)	0.92839	0.927(3)
z[H(2)]	0.67706	0.6766(5)	0.17817	0.17(1)	0.18045	0.187(3)

The three solids crystallize with the space group *Pnma* in an orthorhombic structure with both metal and H atoms in *4(c)* sites and exhibiting (x, 1/4, z) coordinates.

Table 3
Lattice parameters for CaH_2, SrH_2 and BaH_2 calculated using the generalized gradient approximation and pseudopotentials with ("Large core") and without ("Small core") the $(n-1)s$ and $(n-1)p$ semi-core electrons

	CaH_2		SrH_2		BaH_2	
	Large core	Small core	Large core	Small core	Large core	Small core
a (Å)	5.891	5.899	6.081	6.354	6.751	6.812
b (Å)	3.566	3.570	3.699	3.854	4.115	4.150
c (Å)	6.767	6.769	7.031	7.286	7.859	7.836

Large core and small core calculations consider cations with charges of $Q = +2e$ and $+10e$, respectively.

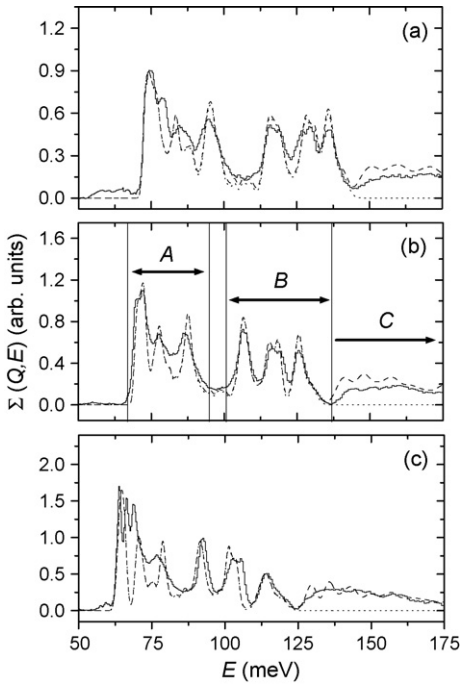

Fig. 5. Comparison between the generalized self-inelastic structure factors derived from the neutron scattering experiments (full line histograms), and from the ab initio simulations (dashed lines). The one-phonon fundamental components of the latter spectra have been also reported (as dotted lines) to mark the end of the phonon density of states. Panels (a), (b) and (c) contain spectra of CaH_2, SrH_2 and BaH_2, respectively. The strontium hydride spectrum is divided into three zones (namely "*A*", "*B*" and "*C*") as explained in the main text.

4. Discussion

Our experimental determinations of the generalized self-inelastic structure factor in orthorhombic alkaline earth hydrides (see Figs. 3 and 5) contain detailed information on the hydrogen self-dynamics in these compounds, especially regarding its dependence on the cation atomic number, *Z*, and on the lattice constants. As we have already mentioned in Section 1, there was no previous high-resolution experimental study available on $\Sigma(Q,E)$ in two of these systems (namely SrH_2 and BaH_2); thus the present work fills a certain gap in the knowledge of the H vibrational dynamics in ionic hydrides. Concerning CaH_2, the present measurement of $\Sigma(Q,E)$ shows an excellent agreement with the recent one from Morris et al. [13], providing a further improvement of the spectral energy resolution.

Looking at Fig. 3 one can immediately distinguish three main spectral areas for all the $HAEH_2$ patterns reported, if the small acoustic part at low energies ($E < 50$ meV) is disregarded. Choosing for example SrH_2 as reference, one observes a three-peak zone from 67 to 95 meV (labeled "*A*"), then a second three-peak zone from 101 to 136 meV (labeled "*B*"), and finally a large hump at $E > 137$ meV (labeled "*C*"). Actually a remarkable feature is represented by the strong similarity among the three generalized self-inelastic structure factors of $HAEH_2$: it suggests that even from the dynamical point of view CaH_2, SrH_2 and BaH_2 can be gathered together in a close group of compounds, unified by their common crystal structure in a way similar to what was found for the heavy alkali metal hydrides: KH, RbH and CsH [27]. Another interesting characteristic of the present phonon spectral data is the softening of both "*A*" and "*B*" optical bands, while the cation atomic number increases, as made even clearer in Fig. 5, where "*A*" moves from the energy range (71–101) to (67–94) meV, while "*B*" from (111–141) to (102–133) meV. In addition, one can observe that "*A*" becomes globally sharper moving from CaH_2 to BaH_2. This effect present in $\Sigma(Q,E)$ has probably to be related to the flatness of the corresponding phonon dispersion curves at the edge of the first Brillouin zone. On the contrary, "*B*" shows no sign of such a shrinking.

In Fig. 5, a detailed comparison between IINS and ABINIT $\Sigma(Q,E)$ curves is also shown and one can easily observe an overall satisfactorily agreement in all cases. However, for BaH_2 the comparison between experiment and simulation, though globally acceptable, does not result as good as for the other two hydrides. For example, the positions and the heights of the second and third peak (at 66.5 and 68 meV, respectively) are not precisely reproduced by ABINIT, and, in addition, all the first three simulated peaks exhibit a certain width, which reveals a slightly too large dispersion of the "*A*" optical phonon bands. Similar differences are also visible in the CaH_2 simulated spectrum, but to a less severe extent. At this stage it is worth reminding, as already mentioned in the previous section, that the simulated $\Sigma(Q,E)$ curves in Fig. 5 have been produced after a slight rigid shift of the ABINIT phonon frequencies, in order to optimize the agreement with the experimental spectra. This procedure (or alternatively the use of a scaling factor) is not at all uncommon in dealing with ab initio vibrational energies [35], and it does not alter the overall spectral shape. Besides, the effect of the experimental energy resolution has been also checked, but found irrelevant in the plotted spectral range ($50\text{ meV} < E < 175\text{ meV}$).

With the help of the ABINIT estimates of the phonon polarization vectors for each individual atom in the CaH_2 lattice cell, it was also possible to test the physical interpretation of the spectral branches "*A*" and "*B*" proposed in ref. [13]. The former lower-energy branch, "*A*", has been associated with the vibration of the H(2) atom, which exhibits an approximately square-pyramidal coordination (i.e. five Ca neighbor atoms) at slightly variable distances, ranging between 2.31 and 2.8 Å [11]. No degeneracy in the localized H(2) wave-function is therefore estimated, and so three similar spectral features, corresponding to three orthogonal axes, are expected [36]. On the contrary, the latter higher energy branch, "*B*", has been connected to the H(1) atom, which shows four nearest neighbor Ca atoms, implying a tetragonal symmetry with distances ranging between 2.16 and 2.5 Å [11]. However, this is an irregular tetrahedron, so one can expect two spectral features with a 2 to 1 intensity ratio [36], but with the more prominent band showing some additional splitting.

In Fig. 6 we have reported the one-phonon component of the generalized self-inelastic structure factor for CaH_2 derived from the present ab initio simulations. The contributions from the two non-equivalent hydrogen atoms, H(2) and H(1), are plotted separately and basically confirm the aforementioned interpretation about the origin of the two branches "*A*" and "*B*". However, some minor discrepancies from the model of ref. [13] emerge: "*B*" shows three well-separated and almost identical peaks, "B_1",

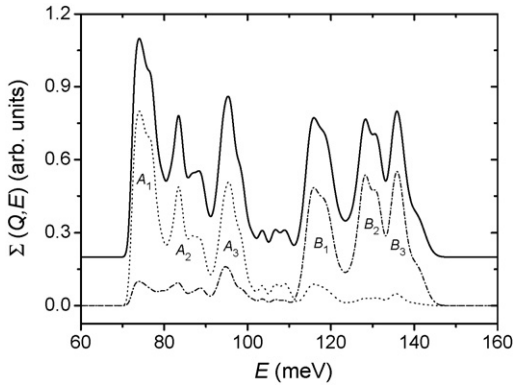

Fig. 6. One-phonon (fundamental) component of the generalized self-inelastic structure factor for CaH_2 derived from ab initio simulations. The contributions from the two non-equivalent hydrogen atoms are plotted separately: dotted line for H(2), and dash-dotted line from H(1). The sum of these two contributions is also reported (thick full line) and vertically shifted for graphical reasons. Symbols "$A_{1,2,3}$"and "$B_{1,2,3}$" are explained in the main text.

"B_2" and "B_3", instead of two peaks with a 2 to 1 intensity ratio; while in "A" one observes that"A_1" is about twice as large as "A_2" and "A_3", and not of the same intensity. In addition, some modest coupling between the motions of tetragonal and square-pyramidal H ions can be observed in the H(1) contribution to "A" and the H(2) contribution to "B". But this is not at all surprising in an ionic compound, which is generally characterized by the existence of long-range inter-atomic interactions, in this case between H atoms placed in different symmetry sites 2.5–3.0 Å apart [11]. As for the third spectral branch, "C", this comes out to be related only to multi-phonon excitations (as shown by the simulated one-phonon components reported in Fig. 5), and consequently it has not been considered in the present discussion.

This kind of study was extended to the other two $HAEH_2$ samples in order to check if the interpretation of ref. [13] was directly extendable to SrH_2 and BaH_2 too. The result was positive, as clearly shown in the two panels of Fig. 7, and, besides, it was possible to note that the small cross-components of the

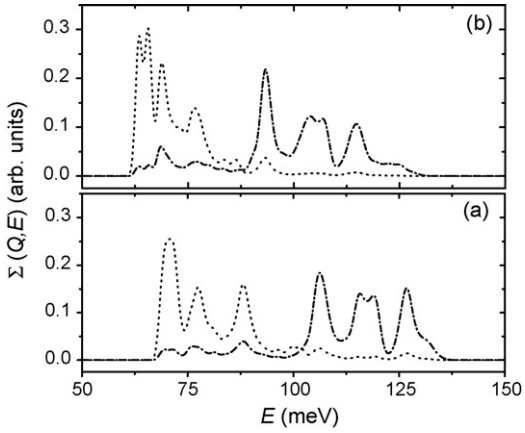

Fig. 7. One-phonon (fundamental) components of the generalized self-inelastic structure factors for SrH_2 (a) and BaH_2 (b), both derived from ab initio simulations. The contributions from the two non-equivalent hydrogen atoms are plotted separately: dotted line for H(2), and dash-dotted line from H(1).

spectral bands "A" and "B" (i.e. the H(1) contribution to "B" and the H(2) contribution to "A") exhibited basically the same magnitude, despite the atomic number of the alkaline earth metal involved, namely 17–19% of H(1) in "A", and 7–8% of H(2) to "B", if areas are considered. This interesting finding seems to support the idea of a direct interaction between H(1) and H(2) sites not mediated by metal atoms.

Finally, together with the phonon energy calculations, ABINIT code has also provided reliable estimates of $HAEH_2$ lattice cell constants and internal coordinates (see Table 2), whose discrepancies from the experimental values [8,10,11] are extremely small, namely of the order of 0.25% (a, b and c) and 0.62% (x and z), and always lower than 0.51% (a, b and c) and 3.52% (x and z), if the dubious experimental value of x[H(2)] for SrH_2 is disregarded [11]. From this point of view one has to consider the ABINIT capability to reproduce the crystal structures of this class of hydrides as totally satisfactory.

5. Conclusion and perspective

In the present paper we have reported incoherent inelastic neutron scattering patterns from orthorhombic alkaline earth hydrides (CaH_2, SrH_2 and BaH_2), measured at $T < 20$ K in the energy and momentum transfer ranges $3\,\text{meV} < E < 500\,\text{meV}$ and $2.8\,\text{Å}^{-1} < Q < 16.5\,\text{Å}^{-1}$ on the TOSCA-II spectrometer. From the medium-energy region of these spectra (namely 63–140 meV, coinciding with the optical phonon bands), we were able to extract accurate generalized self-inelastic structure factors. These experimental physical quantities, which can be directly related to the phonon frequency distributions [27], were then compared to equivalent results obtained from ab initio lattice dynamics simulations, performed via the ABINIT code [29], and based on density functional theory and pseudopotentials. The overall agreement between neutron and ab initio data turned out to be satisfactory, even though some discrepancies still appeared in the first optical phonon zone, especially in the case of barium hydride, where peak positions, heights and widths were not perfectly reproduced by simulations. However, the most interesting result provided by the ABINIT simulations is probably the separation of the spectral contributions coming from the two non-equivalent H atoms in the hydride lattice, namely H(1) and H(2). This gives a strong and quantitative support to the recent physical interpretation of the spectral features proposed by Morris et al. for CaH_2 [13], and is easily extendable to all the orthorhombic alkaline earth hydrides.

Acknowledgements

The skillful technical help of the ISIS User Support Group is gratefully acknowledged. Ab initio results have been obtained through the use of the ABINIT code, a common project of the Université Catholique de Louvain (Belgium) and other contributors. This work has been partially supported by Ente Cassa di Risparmio di Firenze through the Firenze Hydrolab project. AJRC and GDB thank the Center for Molecular Structure and Dynamics (CMSD) for financial assistance for GDB's visit.

References

[1] B. Bogdanović, M. Schwickardi, J. Alloys Compd. 253–254 (1997) 1; B. Bogdanović, R.A. Brand, A. Marjanović, M. Schwickardi, J. Tölle, J. Alloys Compd. 302 (2000) 36.

[2] J.R. Santisteban, G.J. Cuello, J. Dawidowski, A. Fainstein, H.A. Peretti, A. Ivanov, F.J. Bermejo, Phys. Rev. B 62 (2000) 37.

[3] R. Yu, P.K. Lam, Phys. Rev. B 37 (1988) 8730; H.G. Schimmel, M.R. Johnson, G.J. Kearley, A.J. Ramirez-Cuesta, J. Huot, F.M. Mulder, Mater. Sci. Eng. B 108 (2004) 38; H.G. Schimmel, M.R. Johnson, G.J. Kearley, A.J. Ramirez-Cuesta, J. Huot, F.M. Mulder, J. Alloys Compd. 393 (2005) 1.

[4] M. Bortz, B. Bertheville, G. Böttger, K. Yvon, J. Alloys Compd. 287 (1999) L4.

[5] R.W.G. Wyckoff, Crystal Structures, vol. I, Interscience, New York, 1963.

[6] G.S. Smith, Q.C. Johnson, D.K. Smith, D.E. Cox, R.L. Snyder, R.-S. Zhou, A. Zalkin, Solid State Commun. 67 (1988) 491.

[7] E. Zintl, A. Harder, Z. Elektrochem. 41 (1935) 5.

[8] J. Bergsma, B.O. Loopstra, Acta Cryst. 15 (1962) 92; A.F. Andresen, A.J. Maeland, D. Slotfeldt-Ellingsen, J. Solid State Chem. 20 (1977) 93.

[9] N. Brese, M. O'Keeffe, R. Von Dreele, J. Solid State Chem. 88 (1990) 571.

[10] W. Bronger, S. Chi-Chien, P. Müller, Z. Anorg. Allg. Chem. 545 (1987) 69.

[11] T. Sichla, H. Jacobs, Eur. J. Solid State Inorg. Chem. 33 (1996) 453.

[12] G.J. Snyder, H. Borrmann, A. Simon, Z. Kristallogr. 209 (1994) 458.

[13] P. Morris, D.K. Ross, S. Ivanov, D.R. Weaver, O. Serot, J. Alloys Compd. 363 (2004) 85.

[14] A.J. Maeland, J. Chem. Phys. 52 (1969) 3952.

[15] A. El Gridani, M. El Mouhtadi, Chem. Phys. 252 (2000) 1.

[16] A. El Gridani, M. El Mouhtadi, J. Mol. Struct. (Theochem.) 532 (2000) 183.

[17] A. El Gridani, R. Drissi El Bouzaidi, M. El Mouhtadi, J. Mol. Struct. (Theochem.) 531 (2000) 193.

[18] A. El Gridani, R. Drissi El Bouzaidi, M. El Mouhtadi, J. Mol. Struct. (Theochem.) 577 (2002) 161.

[19] H. Smithson, C.A. Marianetti, D. Morgan, A. Van den Ven, A. Predith, G. Ceder, Phys. Rev. B 66 (2002) 144107.

[20] D. Colognesi, M. Celli, F. Cilloco, R.J. Newport, S.F. Parker, V. Rossi-Albertini, F. Sacchetti, J. Tomkinson, M. Zoppi, Appl. Phys. A 74 (Suppl. 1) (2002) 64.

[21] H.H. Paalman, C.J. Pings, J. Appl. Phys. 33 (1962) 2635.

[22] A.K. Agrawal, Phys. Rev. A 4 (1971) 1560; V.F. Sears, Adv. Phys. 24 (1975) 1.

[23] M.M. Bredov, B.A. Kotov, N.M. Okuneva, V.S. Oskotskii, A.L. Shakh-Budagov, Sov. Phys. Solid State 9 (1967) 214.

[24] J. Dawidowski, J.R. Santisteban, J.R. Granada, Physica B 271 (1999) 212.

[25] D. Colognesi, C. Andreani, E. Degiorgi, J. Neutron Res. 11 (2003) 123.

[26] G. Auffermann, G.D. Barrera, D. Colognesi, G. Corradi, A.J. Ramirez-Cuesta, M. Zoppi, J. Phys.: Condens. Matter 16 (2004) 5731.

[27] P.C.H. Mitchell, S.F. Parker, A.J. Ramirez-Cuesta, J. Tomkinson, Vibrational Spectroscopy with Neutrons with Applications in Chemistry, Biology, Materials Science and Catalysis, World Scientific, Singapore, 2005.

[28] R. Baddour-Hadjean, F. Fillaux, N. Floquet, S. Belushkin, I. Natkaniec, L. Desgranges, D. Grebille, Chem. Phys. 197 (1995) 81.

[29] X. Gonze, J.-M. Beuken, R. Caracas, F. Detraux, M. Fuchs, G.-M. Rignanese, L. Sindić, M. Verstraete, G. Zerah, F. Jollet, M. Torrent, A. Roy, M. Mikami, Ph. Ghosez, J.-Y. Raty, D.C. Allan, Comp. Mater. Sci. 25 (2002) 478.

[30] C. Hartwigsen, S. Goedecker, J. Hutter, Phys. Rev. B 58 (1998) 3641.

[31] J.P. Perdew, K. Burke, M. Ernzerhof, Phys. Rev. Lett. 77 (1996) 3865.

[32] G.D. Barrera, D. Colognesi, P.C.H. Mitchell, A.J. Ramirez-Cuesta, Chem. Phys. 317 (2005) 119.

[33] X. Gonze, C. Lee, Phys. Rev. B 55 (1997) 10355.

[34] A.J. Ramirez-Cuesta, Comp. Phys. Commun. 157 (2004) 226.

[35] J.B. Foresman, A. Frisch, Exploring Chemistry with Electronic Structure Methods, second edition, Gaussian, Pittsburgh (PA), 1993.

[36] D.K. Ross, in: H. Wipf (Ed.), Hydrogen in Metals, vol. 3, Springer, Berlin, 1997, p. 153.